Analysis of Coupling Loops in Waveguide and Application to the Design of a Diode Switch

W. C. JAKES, JR., FELLOW, IEEE

Abstract—A voltage-controlled switch using PIN diodes loop-coupled to a section of WR975 waveguide is described. Total switching loss of over 40 dB could be obtained at 960 Mc/s. The switch was operated at rates up to 60 c/s for use in the satellite-tracking radar system at Crawford Hill, N. J. The 3-dB bandwidth of the complete switch was 0.7 Mc/s. The forward switch loss was low enough to permit transmission of 10 kW of 960-Mc/s power with a 50 percent duty cycle without excessive heating of the diodes.

Theoretical analysis of the complete waveguide switch involved determination of the coupling of individual loops to the dominant and higher-order waveguide modes. A reciprocity theorem was used to calculate the appropriate mode coupling coefficients. These were then related to the insertion loss by means of an equivalent circuit for the complete switch. A number of experiments confirmed the theory.

I. Introduction

IN THE DESIGN of a 960-Mc/s satellite-tracking radar system, a problem arose concerning the leakage of transmitter noise into the receiver during the reception period. As shown in Fig. 1, the leakage path involved reflection from the antenna and imperfect balance in the duplexer. The most convenient solution to the problem of attenuating the transmitter noise the required 30 to 40 dB proved to be a switch in the transmitter waveguide, as shown.

The switch as finally evolved is shown in Figs. 2 and 3. It consists of four identical diode switching elements loop-coupled to a rectangular waveguide approximately $3/4\lambda_g$ apart. Figure 4 shows one switching element. The heart of the element is a pair of PIN [1] diodes which can be forward- or back-biased by a modest control voltage to short- or open-circuit a resonant loop coupled to the waveguide, thus introducing a certain amount of switchable attenuation. The combination of a number of these switch elements together with their mutual interactions made it possible to achieve the required characteristics. This paper is concerned with a detailed theoretical and experimental study of the properties of the switch elements and their coupling to the waveguide.

II. Switch Elements

A diagram of one switch element is shown in Fig. 5. The loop which couples to the waveguide is made of #10 copper wire and is one free-space wavelength in circumference. This size proved to give the maximum loss for a given angle of coupling to the waveguide. The diode switch sections contain two PIN diodes in a strip line structure[1] with transitions to 50 ohm coax. at each end. In operation, the diodes can be made to look like a very low or very high resistance by forward or reverse bias. Advantage is taken of this fact by locating the diodes $3/4\lambda$ from the resonant loop so that the loop terminals may be effectively short- or open-circuited. Maximum waveguide transmission loss occurs with the loop short-circuited which, in this case, corresponds to the diodes back-biased. The diode section is followed by an adjustable short-circuited coaxial line in order to antiresonate the residual diode parallel reactance and achieve a high impedance in the back-biased condition. In the low-loss condition the diodes are forward-biased, effectively open-circuiting the coupling loop and reducing its coupling to the waveguide, and also reducing the power incident on the diodes.

In order to obtain some quantitative estimates for the three quantities of interest, namely maximum and minimum transmission loss (in the waveguide) and power incident on the diodes when the transmitter is on, the equivalent circuit shown in Fig. 6 is assumed. Here Z_0 is the (coaxial) impedance terminating the waveguide at the source and load ends, and also the characteristic impedance of the line in the switch element; R_d is the diode resistance; L and C represent the resonant loop coupled to the waveguide dominant mode by an ideal transformer with turns ratio a. It is then easy to derive the following relations.

Power dissipated in diodes:

$$P_d = 4\frac{Z_0}{a^2R_d}\left(1+\frac{Z_0}{a^2R_d}\right)^{-2}P_0. \tag{1}$$

Loss of one switch:

$$L_1^2 = \frac{P_0}{E^2/Z_0} = \left(1+\frac{a^2}{2}\frac{R_d}{Z_0}\right)^2 \tag{2}$$

where

$$P_0 = \frac{E_0^2}{4Z_0}.$$

Other measurements have shown that the effective re-

Manuscript received September 30, 1965; revised December 13, 1965.

The author is with Bell Telephone Laboratories, Inc., Murray Hill, N. J.

[1] The diode switch sections were supplied by M. R. Barber and R. E. Fisher of Bell Telephone Laboratories, Inc., Murray Hill, N. J. This diode switch had been designed and developed by the Microwave Device Department for another radar system application.

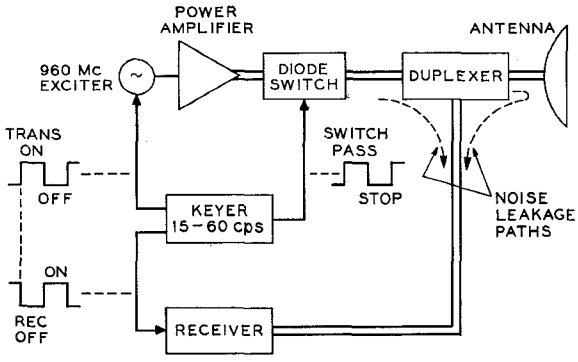

Fig. 1. Block diagram of 960 Mc/s radar.

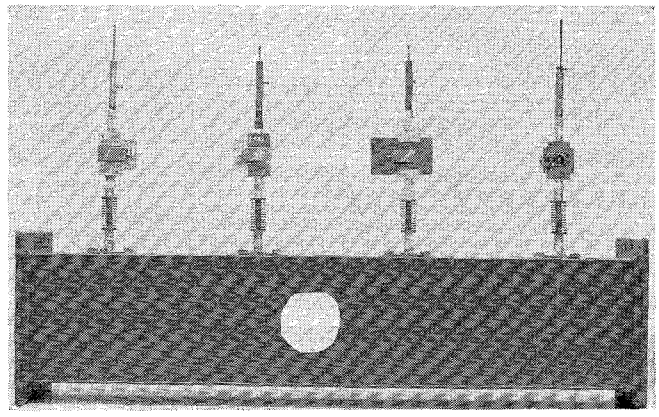

Fig. 2. Photograph of completed switch.

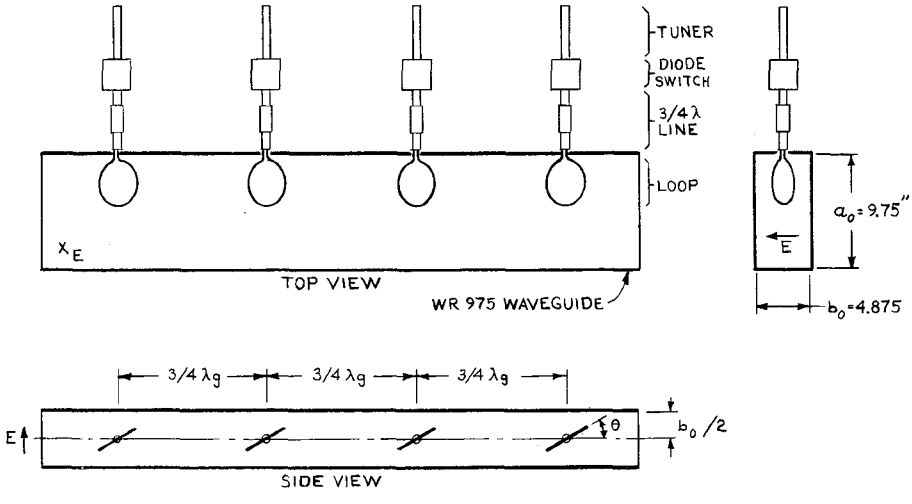

Fig. 3. Diagram of complete switch.

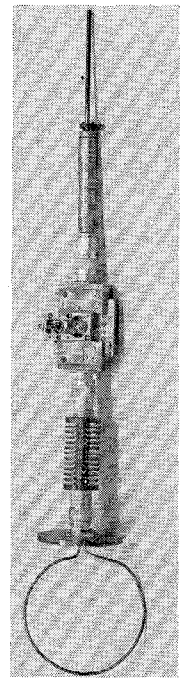

Fig. 4. Photograph of one switch element.

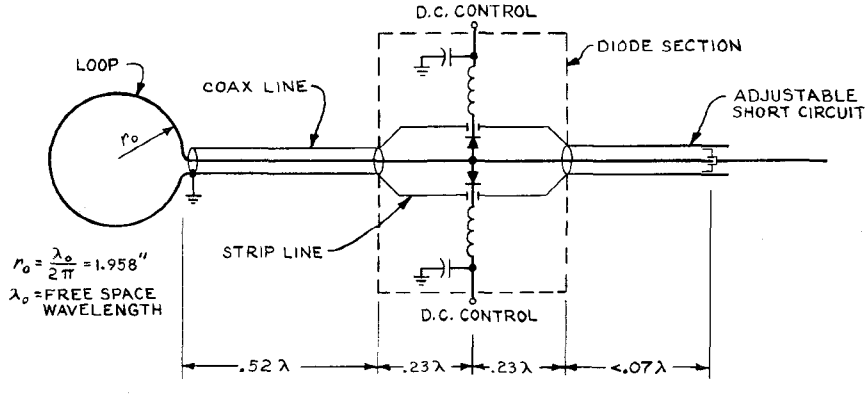

Fig. 5. Diagram of one switch element.

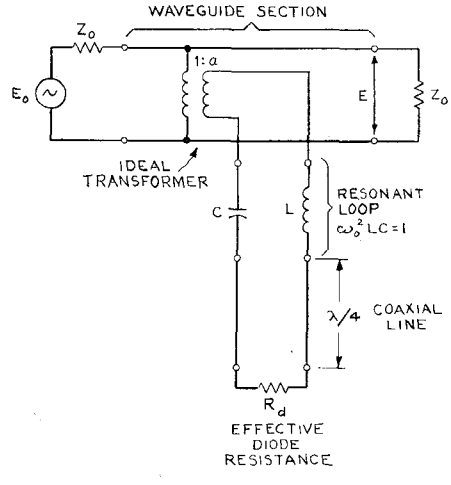

Fig. 6. Equivalent circuit of one switch section coupled to the waveguide.

sistance of the two diodes in parallel is lowered to about 630 ohms by losses in the external circuit in the reverse biased condition. Assuming this value for R_d (reverse), 0.1 ohm for R_d (forward), and $Z_0 = 50$ ohms, (1) and (2) have been evaluated for $0 \leqq a \leqq 1.0$ with the results shown in Table I.

TABLE I

a	Forward loss, dB	Reverse loss, dB	P_d, watts, for $P_0 = 10$ kW
0.0	0.0	0.0	0
0.2	0.00035	2.0	3.2
0.4	0.0014	6.1	13
0.6	0.0031	10.3	29
0.8	0.0056	14.0	51
1.0	0.0087	17.2	80

A total reverse loss of 30 to 40 dB is needed, and thus four switches with $a = 0.6$ should be enough, even neglecting any possible increase in loss due to $\lambda_g/4$ spacing or mutual interactions. For this value of a the forward loss and diode dissipated power with the transmitter on are acceptably low. Circuit losses for the forward-bias case may increase the forward loss, but even an increase in the effective R_d to 1.0 ohm would only increase the forward loss to 0.03 dB for $a = 0.6$.

The equivalent circuit of Fig. 6 assumes that the diode switch section acts as a pure resistive load across the waveguide. Impedance measurements made in the waveguide showed that this was indeed the case over the practical range of $0 \leqq a \leqq 1$. This circuit will therefore be assumed correct, and will be used in the analysis in the following sections.

III. Derivation of Loop Coupling Coefficients

A. General Theory

In general, a current flowing in the switch loop will excite all of the waveguide modes in varying degree. The coupling to the dominant mode is represented by an ideal transformer of turns ratio a (Fig. 6). Coupling to the modes beyond cutoff is of importance only when more than one loop is involved, and in this analysis will be represented by an equivalent mutual reactance between the loops. The assumption is also made that only the dominant TE_{10} mode propagates, and that all other modes are beyond cutoff.

The problem, then, is to calculate the amplitude and phase of all modes of interest in the waveguide due to a given current distribution in the coupling loop for various angles of loop orientation with respect to the waveguide axis. By analogy with the current distribution in a short-circuited two-wire transmission line $\lambda/2$ long, it will be assumed that the current distribution in the loop having a circumference of one wavelength is also sinusoidal with distance around the loop. As shown in Fig. 7, the loop is centered on the mid-point of one-half

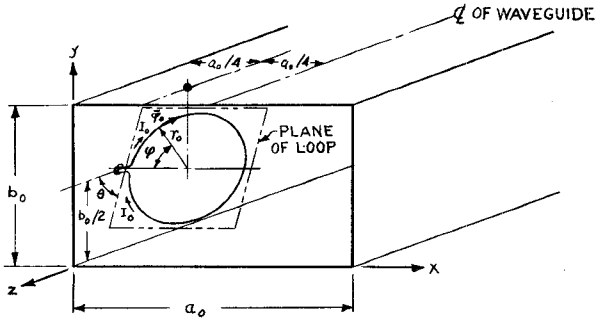

Fig. 7. Orientation of loop in waveguide and coordinate systems.

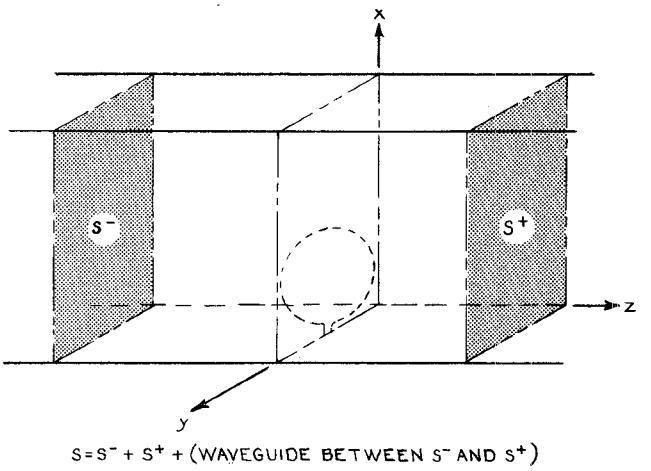

Fig. 8. The surface S.

the waveguide cross section, and lies in a plane making an angle θ with respect to the waveguide axis.

In order to calculate the mode excitation due to the loop current, it is convenient to use a particular reciprocity theorem [2]. Let $\overline{E}_c^{\pm}$, $\overline{H}_c^{\pm}$ be the fields due to a current element of moment $\bar{p} = \bar{I} dl$, and $\overline{E}^{\pm}$, $\overline{H}^{\pm}$ be a known set of source-free fields. The $\pm$ signs refer to fields to the right $(+z)$ or left $(-z)$ of the loop, respectively. The reciprocity theorem then takes the form

$$\int_S (\overline{E}_c \times \overline{H} - \overline{E} \times \overline{H}_c) \cdot d\overline{S} = \overline{E} \cdot \bar{p} \qquad (3)$$

where the surface S completely encloses the current element. Assume also that the fields due to the current element may be expanded in terms of the source-free fields:

$$\overline{E}_c^{\pm} = \sum_{i=0}^{\infty} A_i^{\pm} \overline{E}_i^{\pm}, \qquad \overline{H}_c^{\pm} = \sum_{i=0}^{\infty} A_i^{\pm} \overline{H}_i^{\pm} \qquad (4)$$

where i designates the various modes.

Now let $\overline{E} = \overline{E}_n^{+}$, $\overline{H} = \overline{H}_n^{+}$ where n denotes a particular mode. Let us also take S to be a portion of the waveguide centered on the loop and the cross-section surfaces on either side, as shown in Fig. 8. Since $\overline{E} \times \overline{H} \cdot d\overline{S} = 0$ on a perfect conductor, the integral in (3) need only be evaluated over the waveguide cross

sections S^+ and S^- to the right and left of the loop. Subsitution into (3) then yields:

$$\begin{aligned}\overline{E}_n^+ \cdot \bar{p} = &\int_{S+} [(\sum A_i^+ \overline{E}_i^+) \times \overline{H}_n^+ - \overline{E}_n^+ \\ &\times (\sum A_i^+ \overline{H}_i^+)]_z dS \\ &- \int_{S-} [(\sum A_i^- \overline{E}_i^-) \times \overline{H}_n^+ - \overline{E}_n^+ \\ &\times (\sum A_i^- \overline{H}_i^-)]_z dS. \end{aligned} \tag{5}$$

But

$$\int_S (\overline{E}_i \times \overline{H}_n)_z dS = 0 \qquad \text{for all } i \neq n,$$

thus:

$$\begin{aligned}\overline{E}_n^+ \cdot \bar{p} &= A_n^- \int_{S-} (\overline{E}_n^+ \times \overline{H}_n^- - \overline{E}_n^- \times \overline{H}_n^+)_z dS \\ &= A_n^- G_n^-. \end{aligned} \tag{6}$$

Similarly, by letting $\overline{E} = \overline{E}_n^-$, $\overline{H} = \overline{H}_n^-$, one obtains:

$$\begin{aligned}\overline{E}_n^- \cdot \bar{p} &= A_n^+ \int_{S+} (\overline{E}_n^+ \times \overline{H}_n^- - \overline{E}_n^- \times \overline{H}_n^+)_z dS \\ &= A_n^+ G_n^+. \end{aligned} \tag{7}$$

Thus, the coefficients $A_i^\pm$ can be calculated. The reference set of modes $\overline{E}_n^\pm$, $\overline{H}_n^\pm$ are given in Appendix I. Substitution of these expressions into the integrals of (6) or (7) yields the following.

TE Modes ($n = 1, 2, 3, 5, 7, 9 \cdots$):

$$G_n^\pm = g_n a_0 b_0 \frac{k k_0}{k_c^2} \eta_0 H_{0n}^2, \qquad g_n = \begin{cases} 1: & n = 1, 2 \\ \frac{1}{2}: & n > 2. \end{cases} \tag{8}$$

TM Modes ($n = 4, 6, 8 \cdots$):

$$G_n^\pm = -\frac{1}{2} a_0 b_0 \frac{k k_0}{k_c^2} \frac{1}{\eta_0} E_{0n}^2.$$

The first eight modes are arbitrarily ordered as shown in Table II.

TABLE II

n	Mode	k_1	k_2
1	TE_{10}	π/a_0	0
2	TE_{01}	0	π/b_0
3	TE_{11}	π/a_0	π/b_0
4	TM_{11}	π/a_0	π/b_0
5	TE_{21}	$2\pi/a_0$	π/b_0
6	TM_{21}	$2\pi/a_0$	π/b_0
7	TE_{12}	π/a_0	$2\pi/b_0$
8	TM_{12}	π/a_0	$2\pi/b_0$

Now $\bar{p} = \bar{I} dl$, and $dl = r_0 d\phi$ in terms of the loop coordinates. The coefficient of the nth mode due to $\bar{p}$ is $A_n^\pm$; to get the coefficient due to the total current we must integrate $A_n^\pm$ around the loop:

$$T_n^\pm = \frac{r_0}{G_{n\mp}} \int_0^{2\pi} \overline{E}_{n\mp} \cdot \bar{I} d\phi. \tag{9}$$

Equation (4) then may be rewritten to express the field due to the total current:

$$\overline{E}_c^\pm = \sum_{i=0}^{\infty} T_i^\pm \overline{E}_i^\pm, \qquad H_c^\pm = \sum_{i=0}^{\infty} T_i^\pm \overline{H}_i^\pm. \tag{10}$$

In order to perform the integration in (9), both $\overline{E}$ and $\bar{I}$ must be expressed in the same coordinate system. In terms of the loop coordinates:

$$\begin{aligned}\bar{I} &= I(\phi)\bar{\phi}_0 = I_0 \cos\phi \\ &\quad (\bar{\imath} \sin\phi - \bar{\jmath} \cos\phi \sin\theta + \bar{k} \cos\phi \cos\theta) \end{aligned} \tag{11}$$

where $\bar{\phi}_0$ is a unit vector in the ϕ-direction.

The cartesian coordinates of a point on the loop are:

$$\begin{aligned} x &= r_0(1 - \cos\phi) \\ y &= \frac{b_0}{2} - r_0 \sin\phi \sin\theta \\ z &= r_0 \sin\phi \cos\theta \end{aligned} \tag{12}$$

where r_0 is the loop radius.

Equation (12) enables one to express the fields of the reference modes in the loop coordinates, in order to perform the integrations. The integrand of (9) can thus be written:

$$\begin{aligned}\overline{E}_n^\pm \cdot \bar{I} = [&E_{xn}^\pm(\phi) \cos\phi \sin\phi - E_{yn}^\pm(\phi) \cos^2\phi \sin\theta \\ &+ E_{zn}^\pm(\phi) \cos^2\phi \cos\theta] I_0. \end{aligned} \tag{13}$$

B. Solution for Dominant Mode Coupling

In order to determine the relationship between the turns ratio a and the coupling coefficient $T_1^\pm$ of the dominant mode, an experiment as shown in Fig. 9 is considered. Here a source E_0 with internal impedance Z_0 excites the loop in the waveguide which is terminated at each end in Z_0. The power in one of the loads is then compared to the available power from the source. The equivalent circuit shown in Fig. 9 yields the power in the load (assuming peak values of voltage and current):

$$P = \tfrac{1}{8}(aI_0)^2 Z_0. \tag{14}$$

It is assumed that the waveguide section is long enough so that higher-order modes have decayed to negligible values at the ends. Now the power flow to the right can be expressed in terms of I_0^2 by (9), (10) and (11), relating I_0 to $\overline{E}_1^+$, as will be shown. Assume that $P^+ = R_e I_0^2$, then:

$$R_e I_0^2 = \tfrac{1}{8}(aI_0^2) Z_0,$$

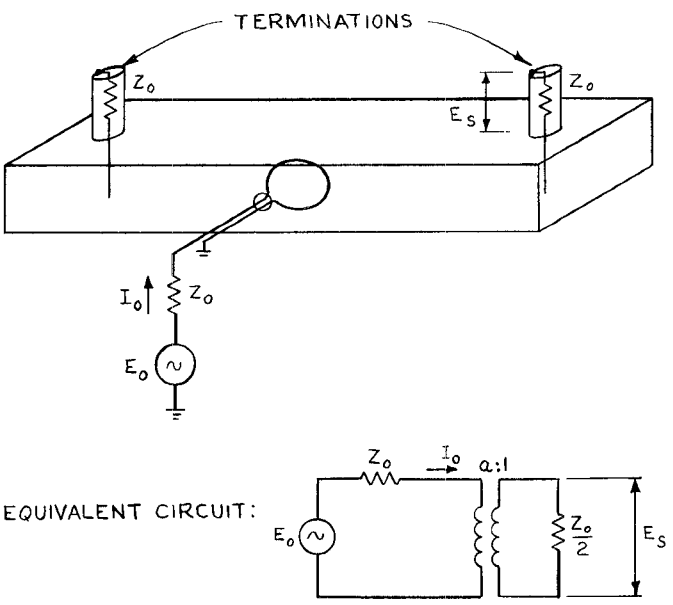

Fig. 9. Experiment to calculate a.

or

$$a = \sqrt{\frac{8R_e}{Z_0}}. \tag{15}$$

R_e will be calculated by the methods outlined in the preceding section.

For the dominant TE_{10} mode, $n=1$ and $k_c=k_1$. Equation (8) gives:

$$G_1^{\pm} = a_0 b_0 \frac{kk_0}{k_1^2}\eta_0 H_{01}^2. \tag{16}$$

Also, from the reference mode listing in Appendix I:

$$\overline{E}_1^- \cdot \overline{I} = E_{y1}^- I_y = i\frac{k_0}{k_1}\eta_0 H_{01} I_0 \sin\theta\cos^2\phi \sin\frac{\pi x}{a_0} e^{ikz}. \tag{17}$$

Thus,

$$T_1^+ = \frac{r_0}{G_1^+}\int_0^{2\pi} E_{y1}^- I_y d\phi = i\frac{2r_0 I_0}{a_0 b_0 H_{01}}\frac{k_1}{k}\sin\theta F(\theta) \tag{18}$$

where

$$F(\theta) = 2\sin\mu\int_0^{\pi/2}\cos(\mu\cos\phi)\cos(\rho\sin\phi)\cos^2\phi d\phi \tag{19}$$

and

$$\mu = \pi\frac{r_0}{a_0}, \qquad \rho = kr_0\cos\theta. \tag{20}$$

In general, the integration must be done numerically; however, for the case $\theta=90°$, $\rho=0$ and an explicit solution is possible:

$$F(90°) = \pi\sin\mu[\Lambda_0(\mu) - \tfrac{1}{2}\Lambda_1(\mu)]. \tag{21}$$

The dominant mode field due to the current in the loop is $E_{cy1}^+ = T_1^+ E_{y1}^+$. Since $H_{cx1}^+ = -E_{cy1}^+/Z_1$, where Z_1 is the wave impedance for the dominant mode, the power flow to the right can be written:

$$P^+ = \frac{1}{2}\int_{S^+}(\overline{E}_{c1}^+) \times (\overline{H}_{c1}^+)^* \cdot \overline{dS}$$

$$= \frac{1}{2Z_1}\int_{S^+} |T_1^+ E_{y1}^+|^2 dS. \tag{22}$$

Substituting the expression for E_{y1}^+ given in Appendix I, and using $Z_1 = \eta_0(k_0/k)$, we obtain

$$P^+ = \frac{kb_0}{2\eta_0 k_0}|T_1^+|^2\int_0^{a_0}\eta_0^2\left(\frac{k_0}{k_1}\right)^2 H_{01}^2\sin^2\frac{\pi x}{a_0}dx \tag{23}$$

$$= \frac{r_0^2}{a_0 b_0}\frac{k_0}{k}\sin^2\theta F^2(\theta)\eta_0 I_0^2. \tag{24}$$

Setting $P^+ = R_e I_0^2$, we obtain the expression for R_e,

$$R_e = \eta_0\frac{r_0^2}{a_0 b_0}\frac{k_0}{k}\sin^2\theta F^2(\theta).$$

Substituting into (15), we finally obtain the expression for the turns ratio,

$$a(\theta) = \frac{r_0}{\sqrt{a_0 b_0}}\sqrt{\frac{8k_0\eta_0}{kZ_0}}\sin\theta F(\theta). \tag{25}$$

Note that $a(-\theta) = -a(\theta)$ since $F(-\theta) = F(\theta)$.

The experiments described later in Section IV were carried out at 960 Mc/s in a waveguide of dimensions $a_0=9.75$ inches, $b_0=4.875$ inches, and with a loop of radius $r_0=1.958$ inches. Additional assumed constants were $\eta_0=377$ ohms, and $Z_0=50$ ohms. The expression for $a(\theta)$ was then evaluated for this particular case by numerical integration and is plotted in Fig. 10, along with the calculated value of coupling loss P^+/P_0. Referring to the equivalent circuit of Fig. 9:

$$\frac{P^+}{P_0} = \frac{(aI_0)^2 Z_0/8}{E_0^2/8Z_0} = \left(\frac{2a}{2+a^2}\right)^2 \tag{26}$$

Measured values of P^+/P_0 are also plotted, and the agreement is reasonably good. A weak point in the analysis is the assumption of a sinusoidal variation in current distribution around the loop, and the difference between theory and experiment may be traceable to departures from this distribution. It is also likely that the current distribution depends to some extent on θ,

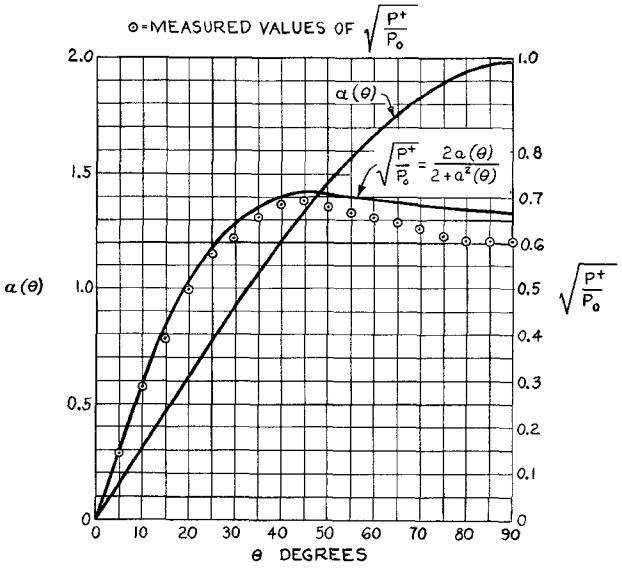

Fig. 10. Variations of a and $P+/P_0$ with θ.

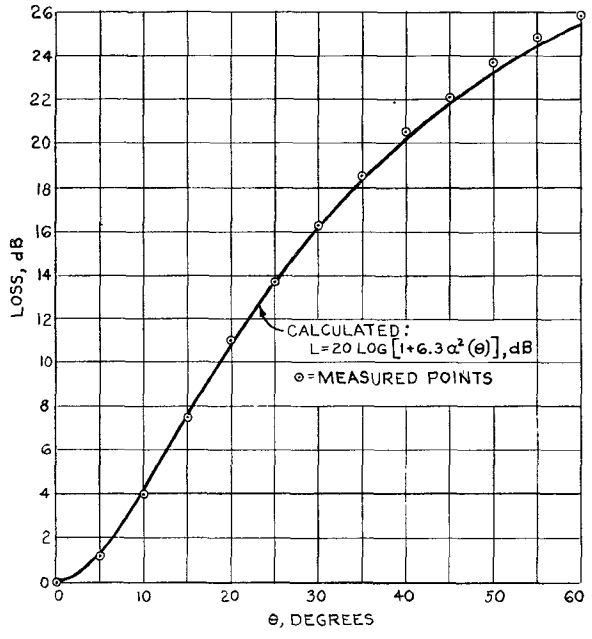

Fig. 11. Loss of one switch section vs. θ.

especially for large values of θ, due to proximity effects of the waveguide walls.

Knowing the variation of a with θ, the switching loss of one switch section for the reverse-biased conductor may be calculated by (2), assuming $R_d = 630$ ohms. The results are shown in the curve of Fig. 11, along with measured points.

C. Solution for Higher-Order Coupling Coefficients

The methods of Section A may be used to calculate $T_n^{\pm}$ for $n>1$ in a manner similar to that for the dominant mode. In this case, however, the quantity of interest is the coupling of one loop to another, which requires calculating first the coupling of the current in one loop to the appropriate waveguide modes and then the voltage induced in the adjacent loop by these modes. Assuming a current I_0 in loop 1, the voltage induced in loop 2 located a distance z_0 to the right of loop 1 may be expressed as follows:

$$E_2 = \sum_{n=2}^{\infty} \oint_{\text{loop 2}} \overline{E}_{cn}^{+} \cdot \overline{dl} = \eta_0 I_0 \sum_{n=2}^{\infty} K_n \tag{27}$$

where

$$\overline{E}_{cn}^{+} = T_n^{+}\overline{E}_n^{+} = \overline{E}_n^{+} \frac{r_0}{G_n^{+}} \oint_{\text{loop 1}} \overline{E}_n^{-} \cdot \overline{I} d\phi. \tag{28}$$

As before, the $\overline{E}_n^{\pm}$ are selected from the set of reference fields listed in Appendix I. Equations (9) and (27) lead to

$$T_n^{+} = \frac{r_0 I_0}{G_n^{+}} \int_{\text{loop 1}}^{2\pi} (E_{xn}^{-} \cos\phi \sin\phi - E_{yn}^{-} \cos^2\phi \sin\theta + E_{zn}^{-} \cos^2\phi \cos\theta) d\phi \tag{29}$$

$$K_n = \frac{T_n^{+} r_0}{\eta_0 I_0} \int_{\text{loop 2}}^{2\pi} (E_{xn}^{+} \sin\phi - E_{yn}^{+} \cos\phi \sin\theta + E_{zn}^{+} \cos\phi \cos\theta) d\phi. \tag{30}$$

The field components in (29) and (30) are to be expressed in terms of ϕ by the coordinate transformation of (12) appropriate to loop 1 or 2. Substituting the appropriate field expressions into (29) and (30) we obtain

$$K_2 = 0 \tag{31}$$

$$\left.\begin{matrix} K_3 \\ K_5 \end{matrix}\right\} = K_E \left(S_1 + \frac{k_1}{k_2} S_4 \sin\theta\right)\left(T_1 - \frac{k_1}{k_2} T_4 \sin\theta\right) \tag{32}$$

$$K_7 = K_E \left(-S_2 + \frac{k_1}{k_2} S_3 \sin\theta\right)\left(T_2 + \frac{k_1}{k_2} T_3 \sin\theta\right) \tag{33}$$

$$\left.\begin{matrix} K_4 \\ K_6 \end{matrix}\right\} = K_M \left[\frac{\alpha}{k_c^2} (-k_1 S_1 + k_2 S_4 \sin\theta) + S_3 \cos\theta\right] \cdot \left[\frac{\alpha}{k_c^2} (k_1 T_1 + k_2 T_4 \sin\theta) + T_3 \cos\theta\right] \tag{34}$$

$$K_8 = K_M \left[\frac{\alpha}{k_c^2} (k_1 S_2 - k_2 S_3 \sin\theta) - S_4 \cos\theta\right] \cdot \left[\frac{\alpha}{k_c^2} (k_1 T_2 - k_2 \sin\theta T_3) + T_4 \cos\theta\right] \tag{35}$$

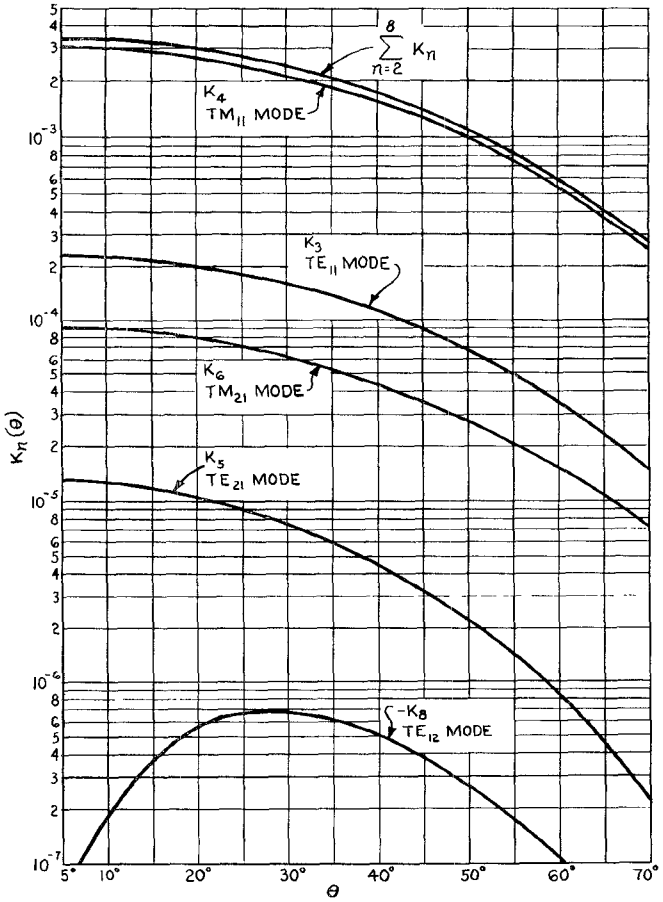

Fig. 12. $Kn(\theta)$.

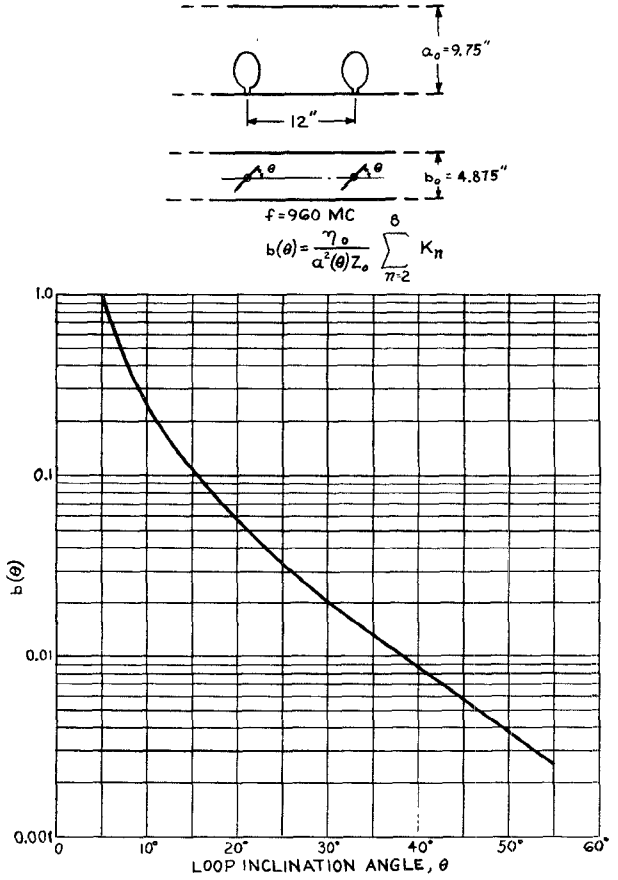

Fig. 13. Normalized mutual reactance between two loops, $b(\theta)$.

where

$$K_E = -i\frac{16r_0^2}{a_0b_0}\frac{k_2^2k_0}{k_c^2\alpha}\sin 2\mu e^{-\alpha z_0} \tag{36}$$

$$K_M = -i\frac{16r_0^2}{a_0b_0}\frac{k_c^2}{\alpha k_0}\sin 2\mu e^{-\alpha z_0} \tag{37}$$

$$\alpha = \sqrt{k_c^2 - k_0^2} = \text{attenuation constant} \tag{38}$$

$$\mu = k_1 r_0. \tag{39}$$

In (31) through (39), the quantities k_1, k_2, k_c, and α are to be expressed appropriately for the given mode (see Table II and Appendix I). The quantities S_i and T_i in (31) through (35) represent definite integrals to be evaluated numerically, and are listed in Appendix II. The K_n have been evaluated as a function of θ and are shown plotted in Fig. 12 for the following particular case:

$a_0 = 9.750$ inches

$b_0 = 4.875$ inches

$\lambda_0 = 12.3$ inches (960 Mc/s)

$r_0 = 1.958$ inches

$z_0 = 12.0$ inches

$\eta_0 = 377$ ohms.

Some features of the K_n are worth noting. There is no TE$_{01}$ coupling ($K_2=0$), and virtually all of the coupling is via the TM$_{11}$ ($n=4$) mode. The coupling thus varies with distance approximately as the amplitude of the TM$_{11}$ mode, which decays at the rate of 4.4 dB/inch for the particular case considered. It is not hard to show that $K_n(\theta) = K_n(-\theta)$ for all K_n considered, as distinct from the dominant mode coupling. Thus, the possibility is raised that the reverse loss of several switches in cascade may be enhanced by utilizing this difference in phase.

A well-known property of the evanescent modes is that no change in phase exists along the waveguide axis. This suggests that the total coupling due to these modes may be expressed as a mutual inductance,

$$E_2 = \eta_0 I_0 \sum_{n=2}^{\infty} K_n = \omega M I_0 = X I_0 \tag{40}$$

where $X=\eta_0\sum K_n$ is the mutual reactance between loops 1 and 2. This reactance is coupled into the waveguide by the turns ratio $a(\theta)$ of the ideal transformer of Fig. 6 as a normalized reactance:

$$b(\theta) = \frac{X}{a^2 Z_0} = \frac{\eta_0}{a^2 Z_0}\sum_{n=2}^{\infty} K_n. \tag{41}$$

The computed variation of $b(\theta)$ is shown in Fig. 13.

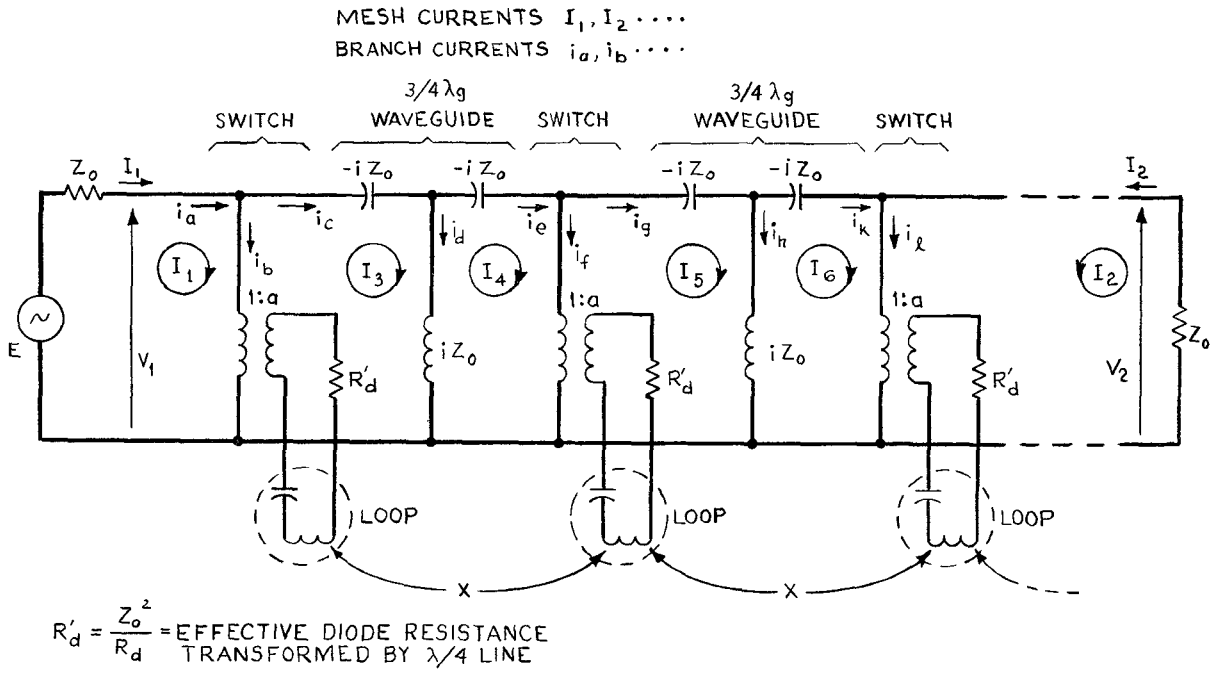

Fig. 14. Equivalent circuit for calculating transmission loss of complete waveguide switch section.

IV. Network Analysis

The most important quantity of interest to calculate is the total transmission loss of several switches in cascade for the reverse-bias condition. A convenient approach is to postulate a circuit equivalent for the waveguide with switches and then use conventional network theory.

A spacing of $\lambda_g/4$ between switches was originally felt to be desirable from the standpoint of obtaining the greatest loss, but physical limitations necessitated increasing the spacing to $3/4\lambda_g$. (As it turned out, this was fortuitous.) The length of waveguide between switches can be represented by a simple T network consisting of reactances. As shown in Fig. 6, each switch can be represented by a resonant loop in series with the transformed diode resistance, $R_d' = Z_0^2/R_d$, coupled across the transmission line by an ideal transformer of turns ratio $a(\theta)$. Each loop is assumed to be coupled to its neighbor by the mutual reactance $X(\theta) = a^2(\theta)b(\theta)Z_0$. (Coupling to loops more distant than the adjacent ones is neglected because of the rapid decay of the higher-order modes.) The resulting equivalent circuit is shown in Fig. 14. Assuming mesh currents I as shown, the transmission loss can then be computed from the solution of the matrix equations by conventional methods. The loss has been calculated as a function of θ for three cases of interest:

1) loops spaced so far apart that the mutual reactance is negligible ($b=0$), but still spaced by an odd multiple of $\lambda_g/4$,

2) loops spaced $3/4\lambda_g = 12.0$ inches apart and all oriented at the same angle θ, and

3) same as Case 2 except loops are alternately oriented at $+\theta$ and $-\theta$.

The calculated values of loss are plotted in Figs. 15, 16, and 17 as functions of the loss L_1 of one switch section alone. Case 1 (no mutual) was computed by setting $b=0$. For Case 3 the mutual coupling between adjacent loops is out of phase with the dominant mode coupling, and thus could be accounted for by replacing b with $-b$. In this case, the mutual coupling can considerably improve the loss if the spacing between loops is such that the mutual coupling is approximately equal to the dominant mode coupling. This only occurs for spacings near $3/4\ \lambda_g$, and explains why this choice was fortuitous as remarked earlier.

V. Experimental Results

A. Measured Switch Loss

The insertion loss of the complete waveguide switch section with two, three, and four switch elements installed was measured as a function of inclination angle θ at 960 Mc/s. The results for the reverse-bias case are plotted in Figs. 15 through 17, and agree well with theory. A spacing of $3/4\ \lambda_g$ was used in all cases except Curve A of Fig. 15. Here the separation between the two loops was $9/4\ \lambda_g$ in order to reduce the mutual coupling to insignificance. A reverse bias of 30 volts was used in all cases.

The insertion loss with the diodes forward-biased was found to be less than 0.1 dB per switch element for $0 \leqq \theta \leqq 25°$, corresponding to loss per individual element of 0 to 14 dB. The forward-bias voltage was set to pro-

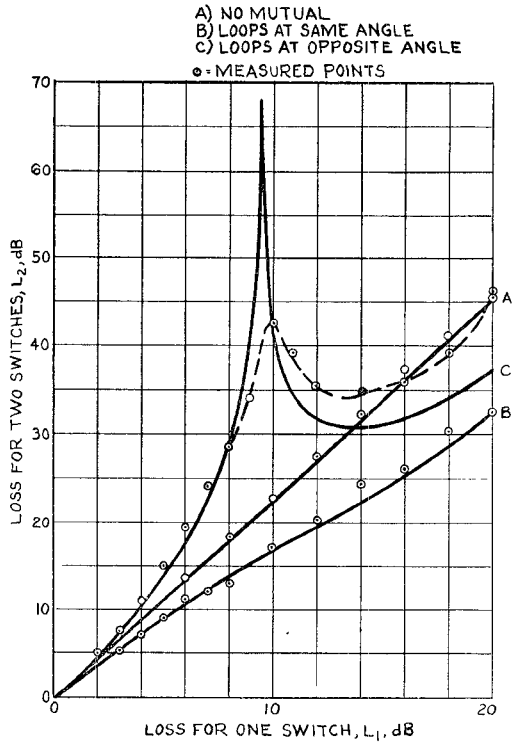

Fig. 15. Calculated and measured loss for two switches.

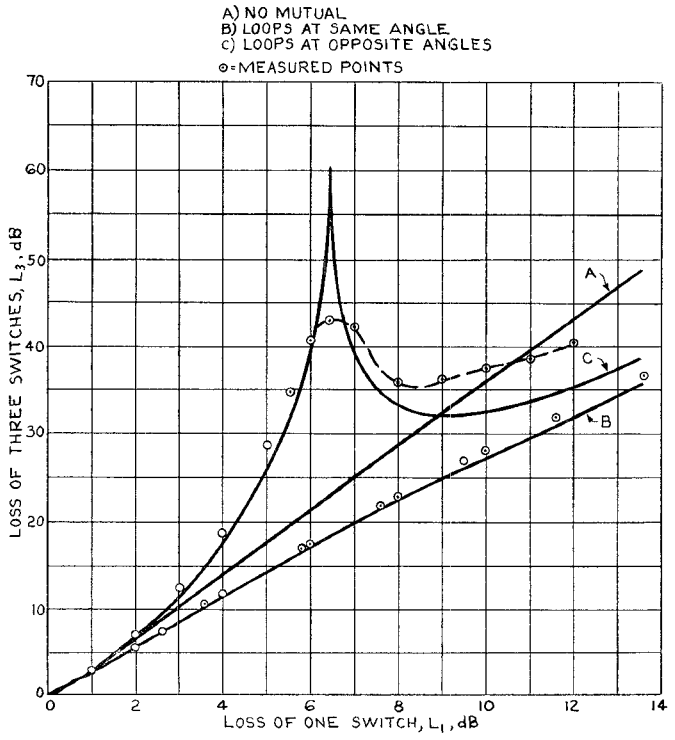

Fig. 16. Calculated and measured loss for three switches.

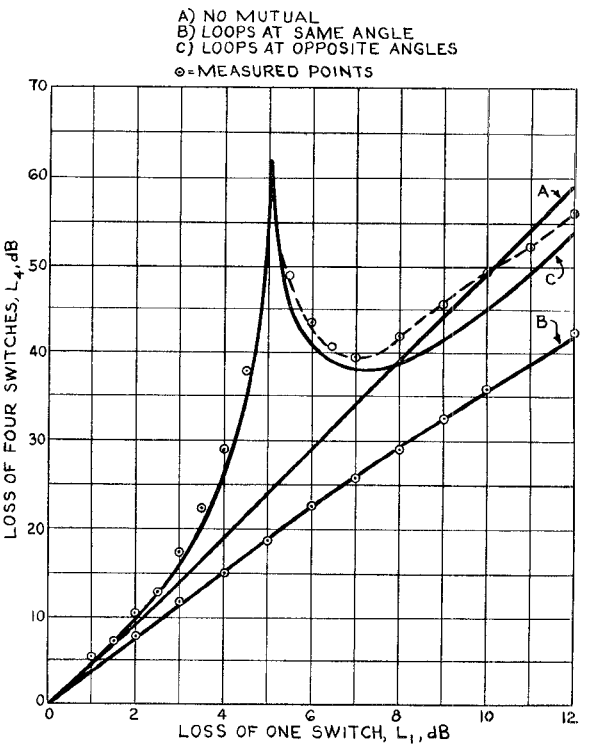

Fig. 17. Calculated and measured loss for four switches.

duce a current of 0.1 amp per diode. Since the final design requirement of 40 dB total loss could be satisfied with four elements, each having an individual loss of less than 5 dB (Curve C of Fig. 17), it was felt that the total forward loss was acceptable. The main objection to higher individual element losses was the possibility of diode damage due to overheating. With 10 kW of CW power flowing through the waveguide, the switch elements were observed to become noticeably, but not dangerously, warm.

B. Two-Loop Coupling

As a final check on the validity of some of the assumptions made for the analysis, and particularly on the variation of coupling with separation, the experiment shown in Fig. 18 was carried out. The insertion loss, defined as the ratio of the power input to loop 1 to that received from loop 2, was measured as a function of the separation z between the loops. Two runs were made, one with the loops at the same angle, $\theta = 10°$, and the other with one loop at $+10°$ and the other at $-10°$. The (voltage) loss may be easily calculated from the equivalent network in Fig. 18:

$$L^{\pm} = \frac{1}{4}\left|\frac{\left(a+\frac{2}{a}\right)^2 - a^2[e^{-j\beta z} \pm j2b(z)]^2}{e^{-j\beta z} \pm j2b(z)}\right| \tag{42}$$

where the $+$ sign refers to the test with the loops

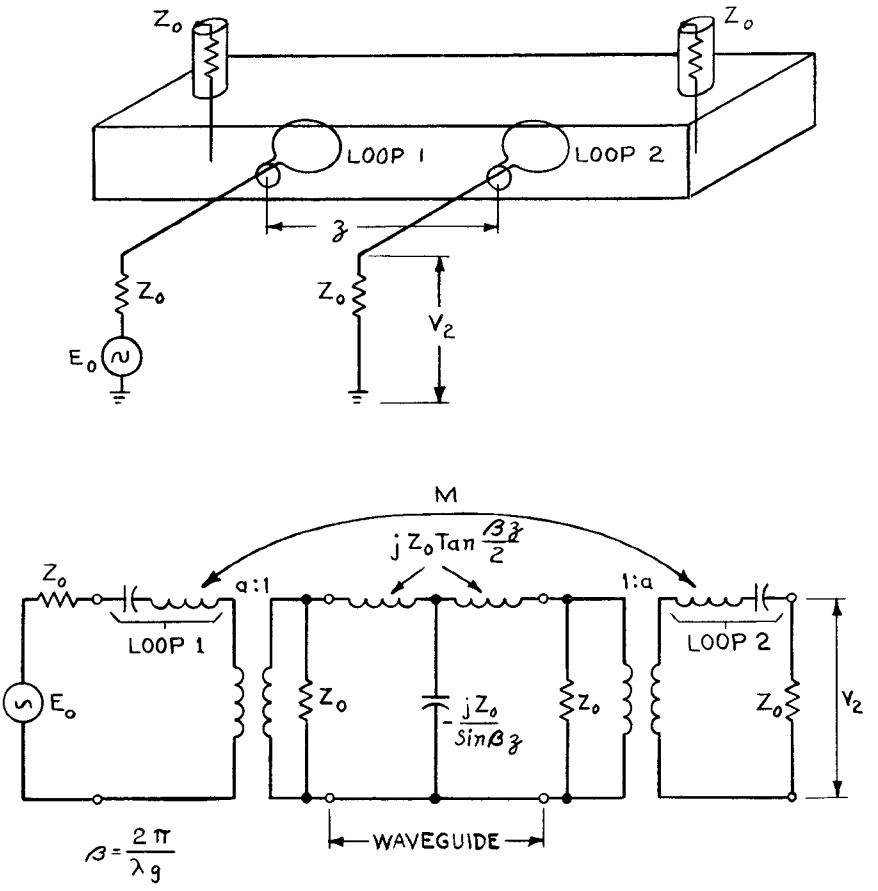

Fig. 18. Two-loop coupling experiment and equivalent network.

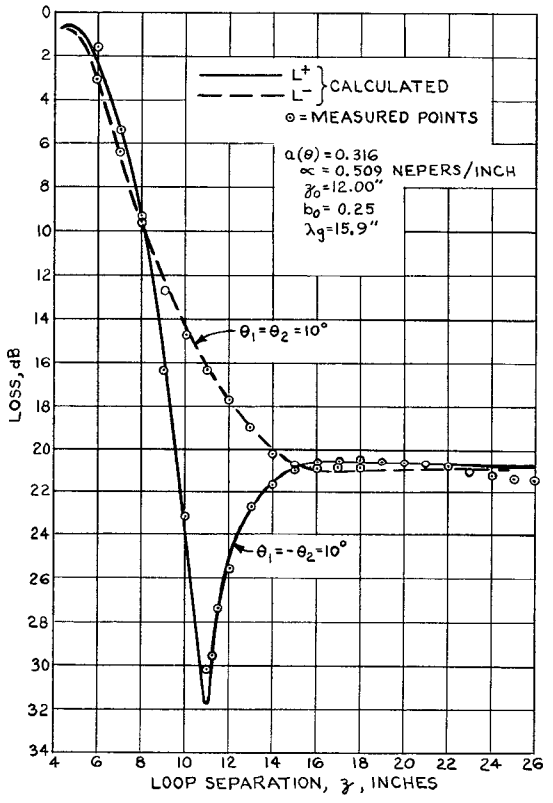

Fig. 19. Calculated and measured loss between two loops.

oriented at the same θ, the $-$ sign to orientation at $+\theta$ and $-\theta$, and $\beta = 2\pi/\lambda_g$. This expression is plotted in Fig. 19 along with the measured points. The mutual reactance term $b(z)$ is now presumed to vary exponentially with z:

$$b(z) = b_0(\theta)e^{\alpha_4(z_0 - z)} \tag{43}$$

where α_4 is calculated for the TM_{11} mode and $b_0(\theta)$ is the value computed previously for spacing z_0 (Fig. 13).

C. Frequency Response

Since there are a number of frequency sensitive elements in the complete switch, it was suspected that the insertion loss would vary significantly with frequency. Two measurements of frequency response were made: 1) a single switch element with 18.2 dB of loss at center frequency, and 2) four swtiches with total loss of 40.8 dB at center frequency. The results are shown in Figs. 20 and 21. It is evident that the four-element switch is only suitable for relatively long radar pulses of 1.5 μs or more. For the present application, however, it is entirely adequate, as the pulses are at least 8000 μs long.

No attempt was made to correlate the measured frequency response with theory, since the Q's of many of the elements were unknown.

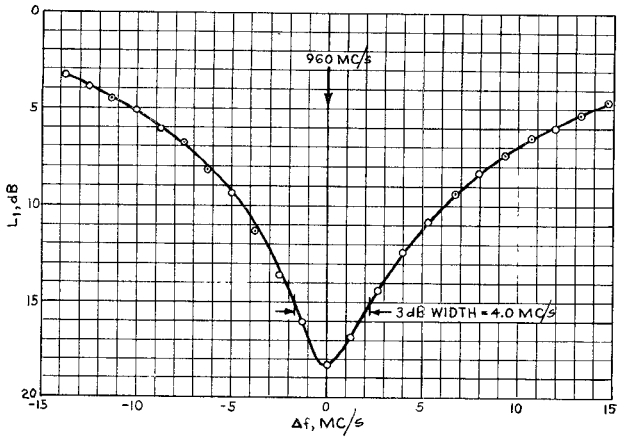

Fig. 20. Frequency variation of the loss of one switching element in the waveguide set for 18.3-dB loss at 960 Mc/s.

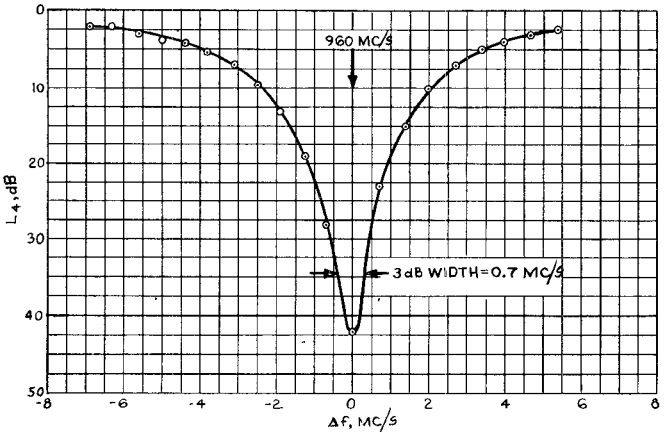

Fig. 21. Frequency variation of the loss of the complete four-element waveguide switch. Loss of each section = 5dB at 960 Mc/s.

Appendix I

Listing of Reference Modes

Coordinate system:

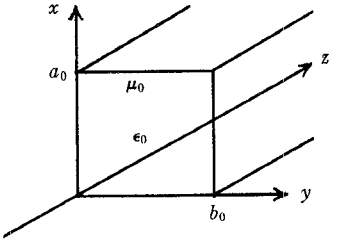

Auxiliary quantities:

$$\eta_0 = \sqrt{\frac{\mu_0}{\epsilon_0}}; \qquad \theta_1 = k_1 x; \qquad \theta_2 = k_2 y$$

$$k_1 = \frac{m\pi}{a_0}; \qquad k_2 = \frac{l\pi}{b_0}$$

$$k_c^2 = k_1^2 + k_2^2; \qquad k_0 = \frac{2\pi}{\lambda_0}; \qquad \lambda_c = \frac{2\pi}{k_c}$$

$$\gamma = ik; \qquad k^2 = k_0^2 - k_c^2; \qquad \lambda_g = \frac{2\pi}{k}.$$

TE_{ml} *Modes*

$$E_x^{\pm} = i\eta_0 \frac{k_0 k_2}{k_c^2} H_0 \cos\theta_1 \sin\theta_2 e^{\mp\gamma z}$$

$$H_y^{\pm} = \pm i \frac{k k_2}{k_c^2} H_0 \cos\theta_1 \sin\theta_2 e^{\mp\gamma z}$$

$$E_y^{\pm} = -i\eta_0 \frac{k_0 k_1}{k_c^2} H_0 \sin\theta_1 \cos\theta_2 e^{\mp\gamma z}$$

$$H_z^{\pm} = H_0 \cos\theta_1 \cos\theta_2 e^{\mp\gamma z}$$

$$H_x^{\pm} = \pm i \frac{k k_1}{k_c^2} H_0 \sin\theta_1 \cos\theta_2 e^{\mp\gamma z}.$$

TM_{ml} *Modes*

$$H_x^{\pm} = i \frac{k_0}{\eta_0} \frac{k_2}{k_c^2} E_0 \sin\theta_1 \cos\theta_2 e^{\mp\gamma z}$$

$$E_y^{\pm} = \mp i \frac{k k_2}{k_c^2} E_0 \sin\theta_1 \cos\theta_2 e^{\mp\gamma z}$$

$$H_y^{\pm} = -i \frac{k_0}{\eta_0} \frac{k_1}{k_c^2} E_0 \cos\theta_1 \sin\theta_2 e^{\mp\gamma z}$$

$$E_z^{\pm} = E_0 \sin\theta_1 \sin\theta_2 e^{\mp\gamma z}$$

$$E_x^{\pm} = \mp i \frac{k k_1}{k_c^2} E_0 \cos\theta_1 \sin\theta_2 e^{\mp\gamma z}.$$

The $\pm$ signs refer to waves traveling towards $\pm z$. A time dependence of $e^{i\omega t}$ is assumed, and the reference magnitudes E_0 and H_0 are peak values.

Appendix II

Integrals involved in higher-order mode coupling:

$$S_1 = \int_0^1 (\sin\psi \cos\zeta \sinh\xi) x dx$$

$$S_2 = \int_0^1 (\sin\psi \sin\zeta \cosh\xi) x dx$$

$$S_3 = \int_0^1 (\cos\psi \cos\zeta \cosh\xi) \sqrt{1 - x^2}\, dx$$

$$S_4 = \int_0^1 (\cos\psi \sin\zeta \sinh\xi) \sqrt{1 - x^2}\, dx$$

$$T_1 = \int_0^1 \cos\psi_1 \cos\zeta_1 \sinh\xi_1 dx$$

$$T_2 = \int_0^1 \cos\psi_1 \sin\zeta_1 \cosh\xi_1 dx$$

$$T_3 = \int_0^1 \sin\psi \cos\zeta \cosh\xi dx$$

$$T_4 = \int_0^1 \sin\psi \sin\zeta \sinh\xi dx$$

$$\psi = \mu\sqrt{1 - x^2}$$

$$\psi_1 = \mu x$$

$$\zeta = \nu x$$

$$\zeta_1 = \nu\sqrt{1 - x^2}$$

$$\xi = \rho x$$

$$\xi_1 = \rho\sqrt{1 - x^2}$$

$$\mu = k_1 r_0$$

$$\nu = k_2 r_0 \sin\theta$$

$$\rho = \alpha r_0 \cos\theta.$$

Acknowledgment

A number of individuals contributed in a variety of ways to the successful completion of this study. R. Kompfner first suggested the possibility of using the diode switch elements. Discussions with C. C. Cutler, S. P. Morgan, and J. R. Whinnery helped with the early stages of design and analysis. E. G. Kimme and P. Liu carried out the computer calculations where required. P. E. Pheffer, R. H. Brandt, and W. E. Legg assisted in the construction and experimental measurements involved.

References

[1] N. G. Cranna, "Diffused silicon PIN diodes as protective limiters in microwave circuits," Tenth Interim Rept., *Microwave Solid State Devices*, U. S. Army Signal Corps, DA-36-039-SC-73224, August 15, 1959.

[2] R. F. Harrington, *Time-Harmonic Electromagnetic Fields*. New York: McGraw-Hill, 1961, pp. 116–118.

An Equivalent Circuit for the "Centipede" Waveguide

T. M. REEDER

Abstract—**An equivalent circuit is presented for the "centipede" coupled-cavity waveguide. The "centipede" waveguide, which is typical of the class of slow-wave structures suitable for use in a wide-band high-power traveling-wave tube, has two pass bands which may interact strongly with a small-diameter electron beam. The equivalent circuit is able to represent both of these pass bands. A detailed comparison with an *S*-band "centipede" waveguide shows that the equivalent circuit can represent the dispersion, interaction, and loss characteristics of the waveguide within a few percent.**

I. Introduction

THE COUPLED-CAVITY waveguide has found extensive use in recent years as a slow-wave circuit in high-power, broadband traveling-wave tubes. Coupled-cavity structures that use resonant coupling elements are a logical choice for high-power tube use because of their rugged construction, relatively high interaction impedance, and large cold bandwidth, often greater than 30 percent [1]. However, analytical studies of tubes using these waveguides are usually tedious because exact electromagnetic field solutions are difficult, even impossible, to obtain. The analysis may be made much simpler if an equivalent circuit can be found to represent the waveguide, but it is difficult to find a simple circuit which will accurately represent the propagation characteristics of broadband waveguides like the "cloverleaf" [1], the "long-slot" [2], and the "centipede" [3] over all operating frequencies.

Equivalent circuits given first by Pierce [4] and later used by Gould [5] and Collier et al. [6] provide an adequate representation of relatively narrow-band waveguides like the "space-harmonic" structure of Chodorow and Nalos [7]. However, the fact that these circuits do not include the effect of intercavity coupling resonance leads to considerable error when they are applied to broadband coupled-cavity waveguides where the cavity and coupling element resonant frequencies may be close together. Curnow [8], [9] has recently shown that by including the coupling element resonance, the dispersion and impedance properties of the "long-slot" waveguide can be accurately represented. Unfortunately, the equivalent circuit must correspond closely to the geometrical configuration of the waveguide as both Curnow and Gittens [10] have demonstrated. The resultant circuit may be quite complicated and difficult to analyze.

The purpose of this paper is to show that one coupled-cavity waveguide, the "centipede," can be accurately represented by a relatively simple equivalent circuit. Waveguides in the "centipede" class have two pass

Manuscript received July 12, 1965; revised January 10, 1966. This research was sponsored by the Air Force Systems Command, Rome Air Development Center, Griffiss Air Force Base, N. Y.

The author is with the Standard Telecommunication Laboratories, Harlow, Essex, England. He was formerly with the W. W. Hansen Laboratories of Physics, Stanford, Calif.